Fluctuating epidemics on adaptive networks

Leah B. Shaw
Department of Applied Science, College of William and Mary, Williamsburg, Virginia 23187, USA

Ira B. Schwartz
US Naval Research Laboratory, Code 6792, Nonlinear Systems Dynamics Section, Plasma Physics Division, Washington, DC 20375, USA

(Received 3 January 2008; published 3 June 2008)

A model for epidemics on an adaptive network is considered. Nodes follow a susceptible-infective-recovered-susceptible pattern. Connections are rewired to break links from noninfected nodes to infected nodes and are reformed to connect to other noninfected nodes, as the nodes that are not infected try to avoid the infection. Monte Carlo simulation and numerical solution of a mean field model are employed. The introduction of rewiring affects both the network structure and the epidemic dynamics. Degree distributions are altered, and the average distance from a node to the nearest infective increases. The rewiring leads to regions of bistability where either an endemic or a disease-free steady state can exist. Fluctuations around the endemic state and the lifetime of the endemic state are considered. The fluctuations are found to exhibit power law behavior.

DOI: 10.1103/PhysRevE.77.066101 PACS number(s): 89.75.Hc, 87.10.Mn

I. INTRODUCTION

The study of recurrent epidemics has a long history [1], and many models, both deterministic and stochastic, have been considered. Deterministic models have been used since the time of Bernoulli and have explained some of the mechanisms in the spread of infectious diseases. However, deterministic models are not sufficient to account for some of the important stochastic dynamics, such as extinction [2,3] and sustained fluctuations [4]. From the general theory of finite Markov chains [5], it was shown that in stochastic models the probability of extinction is equal to one in the asymptotic time limit. Numerical [6–8] and analytic [9] comparisons of stochastic and deterministic models have been performed. The numerical results hold for very small amplitude noise as well as real finite noise. Deterministic susceptible-infective-susceptible (SIS) or susceptible-infective-recovered-susceptible (SIRS) models result in an equilibrium endemic presence of infectives for an appropriate choice of parameters. It is clear that stochastic effects may result in very different dynamics from deterministic models, particularly when fluctuations and/or extinction occur.

More recently, the study of fluctuations and the spread of simple models of epidemics have been simulated on large networks [10–14]. In almost all of these network models, the epidemic propagates on a fixed network. The epidemic dynamics is typically studied as an SIS or SIR model, in which the population is large and isolated. In addition to the dynamics on such fixed architectures, controls based on vaccination have been considered as well [15,16]. Several recent models have considered epidemics on a network that changes structure dynamically according to rules that do not depend on the nodes' epidemic status [17,18].

In contrast to the models of a static network or models with externally applied changes in structure, a new class of models based on endemic SIS populations on an *adaptive* network has been recently introduced [19]. Changes to the network structure are made in response to the epidemic spread and in turn affect future spreading of the epidemic. Here, the governing parameter is one that describes the rewiring rate of the network, which is controlled by the fraction of susceptible (S)-infective (I) links. The network alters dynamically when there are contacts between S and I, and social pressures (the desire to avoid illness) rewire the contacts to be instead between S and S. Infections are reduced due to isolation, and for appropriate choices of parameters, bistability between the disease-free equilibrium and endemic state has been observed. This is in contrast to static networks in a large population, where there is typically only a single attracting endemic or disease-free state. A different model has been introduced in which susceptible-infective links are broken (rather than rewired) and later reconnect at random; this rule for network adaptation also leads to bistability and other dynamics not observed in static network models [20].

In this paper, we introduce a recovered, immune class and consider this slight generalization of the SIS model on an adaptive network. We examine the structure of the network and the dynamics of the fluctuations of the epidemic. Our approach is to combine Monte Carlo simulations and stochastic mean field models for epidemic evolution on evolving networks. The layout of the paper is as follows. We introduce the model in Sec. II and present its bifurcation structure in Sec. III. Properties of the network structure are discussed in Sec. IV. We discuss dynamical properties of the system, including fluctuations and lifetimes of the states, in Sec. V.

II. MODEL

We study a susceptible-infective-recovered-susceptible (SIRS) model on an adaptive network. Epidemic dynamics on the nodes is as follows. The rate for a susceptible node to become infected is $pN_{I,\mathrm{nbr}}$, where $N_{I,\mathrm{nbr}}$ is the number of infected neighbors the node has. The recovery rate for an infected node is r. A recovered node becomes susceptible

again with rate q, which we define as the resusceptibility rate.

While the epidemic spreads, the network is also being rewired adaptively. If a link connects a noninfected node to an infected node, that link is rewired with rate w to connect the noninfected node to another randomly selected noninfected node. Self-links and multiple links between nodes are disallowed.

In examining steady state solutions, it is sufficient to fix one of the rates, as time may be rescaled accordingly. For this reason, we fix $r=0.002$ throughout this paper.

We performed Monte Carlo simulations of this model on a system with $N=10^4$ nodes and $K=10^5$ links. (Larger system sizes with the same node-to-link ratio were also considered. The major results of this paper do not depend strongly on system size.) In each Monte Carlo step (MCS), we randomly select N nodes and M links, where M is the number of links that may potentially rewire (susceptible-infected and recovered-infected links), and the links are selected from the pool of links that may rewire. Initial conditions are constructed in one of two ways. We either generate a random (Erdös-Rényi) graph of susceptibles and convert a fraction f of them to infectives, or we use the final state of a previous run as an initial condition. Transients are discarded and simulations run long enough that the initial conditions do not affect the results.

Following [19], we also developed a corresponding mean field model for the system. The mean field model tracks the dynamics of both nodes and links. P_A denotes the probability of a node to be in state A, where A is either S (susceptible), I (infected), or R (recovered). P_{AB} denotes the probability that a randomly selected link connects a node in state A to a node in state B. We obtain the following mean field equations for the evolution of the nodes:

$$\dot{P}_S = qP_R - p\tfrac{K}{N}P_{SI}, \tag{1}$$

$$\dot{P}_I = p\tfrac{K}{N}P_{SI} - rP_I, \tag{2}$$

$$\dot{P}_R = rP_I - qP_R. \tag{3}$$

For example, in the first equation, recovereds are converted to susceptibles with rate q, and infection spreads with rate p along each susceptible-infected link. Rewiring does not appear directly in the node equations, since rewiring operates on links, but it affects the system implicitly through the number of susceptible-infected links (KP_{SI}). We next write a system of mean field equations for the links. To close the system, we follow [19] and make the assumption for three point terms that $P_{ABC} \approx P_{AB}P_{BC}/P_B$. This assumption leads to the following system of equations for links:

$$\dot{P}_{SS} = qP_{SR} + w\frac{P_S}{P_S+P_R}P_{SI} - 2p\frac{K}{N}\frac{P_{SS}P_{SI}}{P_S}, \tag{4}$$

$$\dot{P}_{SI} = 2p\frac{K}{N}\frac{P_{SS}P_{SI}}{P_S} + qP_{IR} - rP_{SI} - wP_{SI} - p\left(P_{SI} + \frac{K}{N}\frac{P_{SI}^2}{P_S}\right), \tag{5}$$

$$\dot{P}_{II} = p\left(P_{SI} + \tfrac{K}{N}\frac{P_{SI}^2}{P_S}\right) - 2rP_{II}, \tag{6}$$

$$\dot{P}_{SR} = rP_{SI} + w\frac{P_R}{P_S+P_R}P_{SI} + 2qP_{RR} - qP_{SR} - p\tfrac{K}{N}\frac{P_{SI}P_{SR}}{P_S} + w\frac{P_S}{P_S+P_R}P_{IR}, \tag{7}$$

$$\dot{P}_{IR} = 2rP_{II} + p\frac{K}{N}\frac{P_{SI}P_{SR}}{P_S} - qP_{IR} - rP_{IR} - wP_{IR}, \tag{8}$$

$$\dot{P}_{RR} = rP_{IR} - 2qP_{RR} + w\frac{P_R}{P_S+P_R}P_{IR}. \tag{9}$$

The ordinary differential equations of the mean field model can be integrated easily with any well-known numerical integration technique. We choose initial conditions so that we are near an endemic state. We also note that the model does support solutions with negative values, but these are unphysical, and so we ignore them. In the case of stochastic simulations, we have considered the effects of both internal fluctuations, modeled as multiplicative noise, as well as external fluctuations, modeled as additive noise. We use a fourth order Runge-Kutta solver for each of these cases to generate stochastic stimulations of the mean field. The noise strength was kept small for both additive and multiplicative cases, and our stochastic studies were run on stable endemic branches which were far from the disease-free state compared to the noise levels considered. Thus fluctuations in the variables did not drive them to unphysical values for the parameters used here. We also tracked the steady states as a function of parameters using a continuation package [21].

III. BIFURCATION STRUCTURE

We first consider the steady state bifurcation structure of the model. In Fig. 1, we show examples of the average infected fraction versus the transmission rate p. Two steady states can occur, a disease-free state and an endemic state. In the absence of rewiring [Fig. 1(a)], the disease-free state loses stability for very small transmission rates, and only the endemic state is observed at larger p values. When rewiring is introduced [Fig. 1(b)], the disease-free state is stabilized for larger p values. A region of bistability, in which both endemic and disease-free states are observed, now occurs. Bistability was observed previously for the SIS model [19]. Monte Carlo simulation points in Fig. 1 were computed as follows. To locate the upper branches (endemic state), we swept p from larger to smaller values, using the final state of each run as the initial state for the next run. 5×10^3 MCS of transients were discarded, and the steady state was averaged over 10^4 MCS. To locate the lower branch (disease-free state), we began with a randomly connected network in which a fraction f of the nodes were infected, while the rest were susceptible. The system was simulated for 2×10^4 MCS. f values between 0.025 and 0.9 were tried, and at least five runs were done for each p value. If the epidemic died

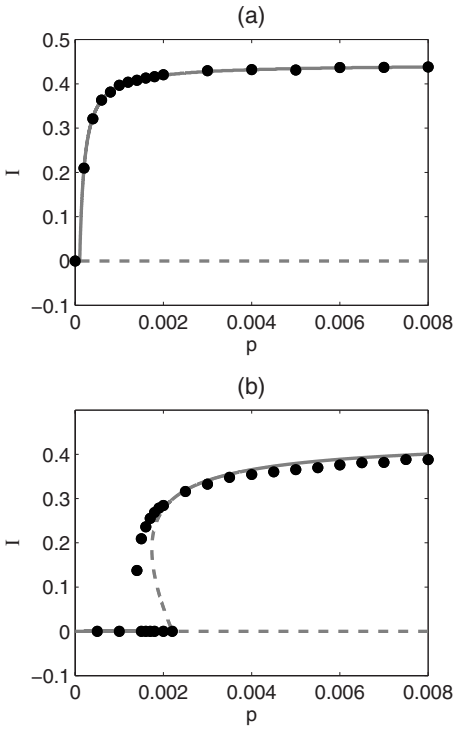

FIG. 1. Average infected fraction vs transmission rate p. (a) Static network, $w=0$. (b) Rewired network, $w=0.04$. Black dots: Monte Carlo simulations; solid gray lines: mean field solution (stable branches); and dashed gray lines: mean field solution (unstable branches). $q=0.0016$, $r=0.002$.

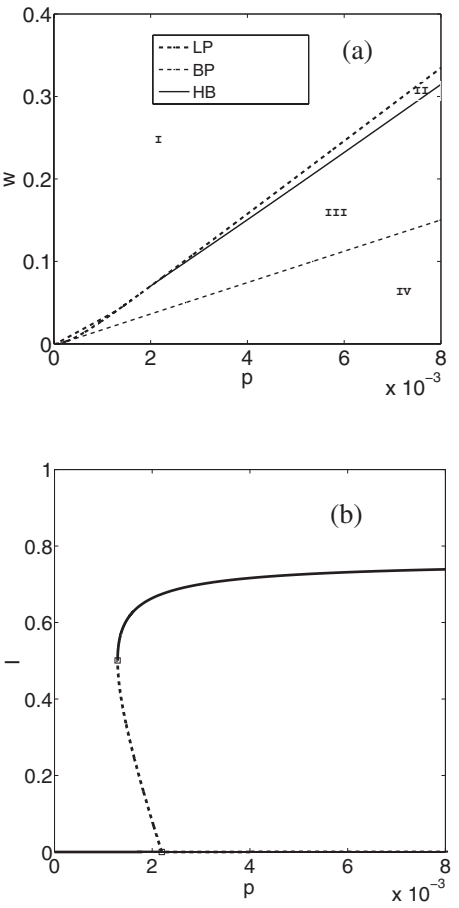

FIG. 2. (a) Two parameter plot for w and p of the bifurcation points for steady states when $q=0.0064$. The heavy dashed line is the line of saddle-node points (limit points). The solid line denotes the Hopf bifurcation points, and the light dashed line denotes the transcritical bifurcation points (BP). (b) A bifurcation diagram of the infective fraction as a function of p, where $w=0.04$. The squares denote the saddle-node point and transcritical point. Dashed lines are unstable branches.

out in any of the runs, the disease-free state was considered stable. Due to the stochastic nature of the Monte Carlo simulation, and because the disease-free state is absorbing, stability designations are uncertain. It is difficult to distinguish a weakly unstable state from a weakly stable state with a short lifetime. Lifetimes of the endemic state are considered in more detail in Sec. V.

The results in Fig. 1 show fairly good agreement between the mean field approximation and the Monte Carlo simulation of the full system, and we typically see this level of agreement in the steady state values, although as we discuss later, the stability and type of bifurcation sometimes differs. Using the mean field model, we next explore the bifurcation structure of the system for a wider range of parameters.

An interesting property of the steady state instabilities appears when one considers each of the steady state bifurcation points of the mean field equations. (There do exist branches of periodic orbits, but since they occur within a very small range of parameters, we ignore them in this paper. They will be treated elsewhere.) If the resusceptibility rate q is held fixed and a bifurcation diagram constructed, we find the existence of at least two distinct regimes for different q values, illustrated in Figs. 2 and 3. The instabilities appear as a transcritical bifurcation from the disease-free steady state, a saddle-node bifurcation of endemic steady states, and a Hopf bifurcation, from which a branch of subcritical unstable periodic orbits emanates (not shown).

In the case where $q=0.0064$, depicted in Fig. 2(b) for $w=0.04$, we show a typical bifurcation plot of stable and unstable steady states as the infection rate p is increased. The dashed lines represent the unstable steady states, while the solid lines depict the attractors. For low values of p the disease-free steady state is stable. Tracking along the disease-free branch, at a critical value of p, an unstable branch (subcritical) of endemic steady states appears. The endemic branch becomes stable at the saddle-node point. There exists a clear region of bistability with coexisting endemic and disease-free states for a range of p. If we now vary the parameter w and track each bifurcation curve, we obtain the result in Fig. 2(a). We describe the bifurcation regions in detail for w larger than 0.1. In region I, we have only a stable disease-free equilibrium. As we cross into region II for large w, the disease-free equilibrium is stable, and there exists an unstable endemic state. Region III exhibits bistability between the disease-free equilibrium and endemic state, and region IV has just a stable endemic equilibrium. We note that at $w=0.04$, we have the simple saddle-node transition depicted in Fig. 2(b), since there is no Hopf bifurcation to periodic cycles at that particular w value.

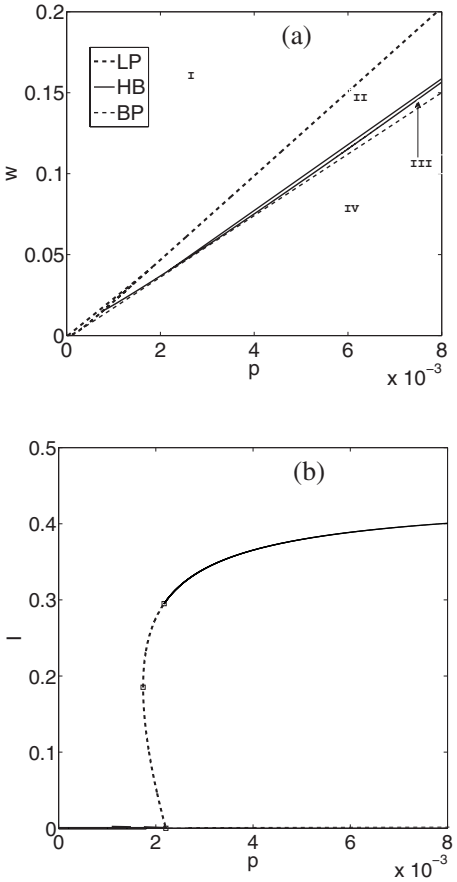

FIG. 3. (a) Two parameter plot of the steady state bifurcation points when $q=0.0016$. The heavy dashed line is the line of limit points. The solid line denotes the Hopf bifurcation points, and the light dashed line denotes the transcritical bifurcations. (b) A bifurcation diagram of the infective fraction as a function of p, where $w=0.04$ (same bifurcation diagram in Fig. 1).

The previous discussion presented a case for resusceptibility rate q where the limit (saddle-node) and Hopf bifurcation branches are close to each other. The distinction between the saddle-node and Hopf branches can be seen more easily if q is lowered to 0.0016, as shown in Fig. 3(a). In Fig. 3(a), for sufficiently large w, as p is increased in region I the system first undergoes a limit point bifurcation, and then a Hopf bifurcation as it passes through region II. The Hopf curve is actually a closed isola in two parameters. The limit point here is a saddle-saddle point, where a steady state having a two-dimensional unstable manifold connects to a steady state with a one-dimensional unstable manifold. In both cases, we have bistable behavior for w sufficiently large, but the region of bistability is much smaller since the Hopf and transcritical branches are closer together for this value of q (region III).

For $w=0.04$, the mean field endemic steady state loses stability in a saddle-node bifurcation for $q=0.0064$ and in a Hopf bifurcation for $q=0.0016$. In our discussion of fluctuations in the endemic state in Sec. V, we will refer to $q=0.0064$ because the saddle-node bifurcation structure best corresponds to the scaling of fluctuations that we observe in Monte Carlo simulations of the full system.

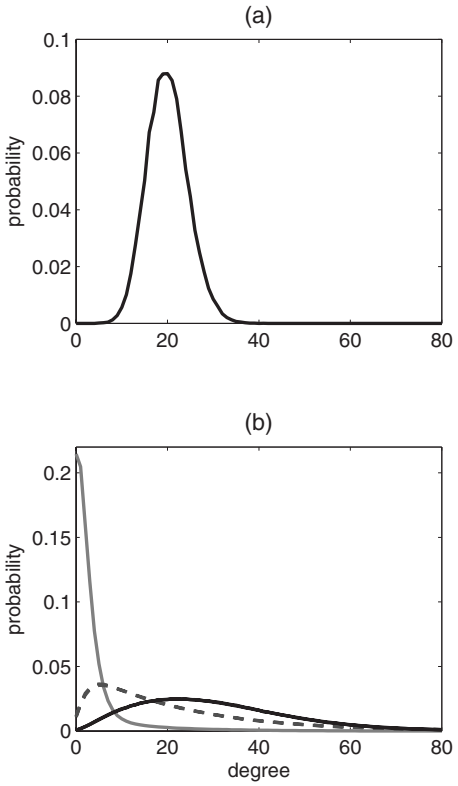

FIG. 4. Degree distributions from Monte Carlo simulation for $p=0.002$, $q=0.0016$, and $r=0.002$. (a) Static network, $w=0$. All node types have Poissonian degree distribution. (b) Rewired network, $w=0.04$. Solid gray line: infectives; dashed line: recovereds; and black line: susceptibles.

IV. NETWORK GEOMETRY

A. Degree distributions

Rewiring leads to significant alterations in the network structure. We first consider the degree distribution. Figure 4 shows degree distributions for each type of node in the absence [Fig. 4(a)] and presence [Fig. 4(b)] of rewiring. In Fig. 4(b), we averaged over 3×10^4 MCS. In Fig. 4(a), the network is static, so we averaged over ten separate runs to obtain better statistics.

Using mean field ideas, we can understand the recovered and susceptible degree distributions as nodes flow from infected to recovered to susceptible. We outline the calculation briefly here. However, this approach does not accurately predict the degree distribution for infected nodes because correlations play a more important role for these nodes, as we will explain below. For this reason, we cannot write a self-consistent set of equations for the degree distributions that could be solved without inputting simulation results.

Let $d_{X,n}$ be the number of nodes in state X (either S, I, or R) with degree n. Recovered nodes originate when infectives recover and are lost when they become susceptible again. The degree of a recovered node can only increase, as other susceptible and recovered nodes wire to connect to it. This leads to the following equations for $d_{R,n}$:

$$\frac{d}{dt}(d_{R,0}) = rd_{I,0} - qd_{R,0} - kd_{R,0},$$

$$\frac{d}{dt}(d_{R,n}) = rd_{I,n} - qd_{R,n} - kd_{R,n} + kd_{R,n-1} \quad \text{for } n > 0, \tag{10}$$

where k is the average rate for nodes to rewire to a given noninfected node. k is given by the ratio of the total rewiring rate to the number of potential target nodes:

$$k = \frac{wK(P_{SI} + P_{IR})}{N(P_S + P_R)}. \tag{11}$$

Given the degree distribution of the infectives $d_{I,n}$ and the probabilities appearing in k, Eqs. (10) can be solved for the degree distribution of the recovereds.

Susceptible nodes originate when recovereds become susceptible again, and they may be lost when they become infected by a neighbor. As with the recovereds, the degree of a susceptible increases due to rewiring. Thus the time evolution of the degree distribution for the susceptibles can be written as

$$\frac{d}{dt}(d_{S,0}) = qd_{R,0} - kd_{S,0},$$

$$\frac{d}{dt}(d_{S,n}) = qd_{R,n} - k'nd_{S,n} - kd_{S,n} + kd_{S,n-1} \quad \text{for } n > 0, \tag{12}$$

where k' is the infection rate per link into a susceptible node. We assume that k' is independent of degree, which we know from simulations is approximately correct (cf. Fig. 5), and write

$$k' = p\frac{P_{SI}}{P_{SI} + P_{SR} + 2P_{SS}}, \tag{13}$$

where the fraction is the ratio of the number of links that can transmit infection to the total number of links into a susceptible. As with the recovereds, the steady state degree distribution for susceptibles can be computed from Eq. (12). The predicted degree distributions for susceptibles and recovereds are overlaid on the actual distributions in Fig. 4(b), using Monte Carlo simulation averages for the infective degree distribution and the node and link probabilities. (Note that the node and link probabilities could instead be obtained from the mean field system.) Deviations between the prediction and simulation are smaller than the width of the curves in Fig. 4(b), so they are indistinguishable.

The degree of infected nodes, however, cannot be predicted by this approximate procedure. We might expect that

$$\frac{d}{dt}(d_{I,0}) = k''d_{I,1} - rd_{I,0},$$

$$\frac{d}{dt}(d_{I,n}) = k''(n+1)d_{I,n+1} - k''nd_{I,n} + k'nd_{S,n} - rd_{I,n} \quad \text{for } n > 0, \tag{14}$$

where

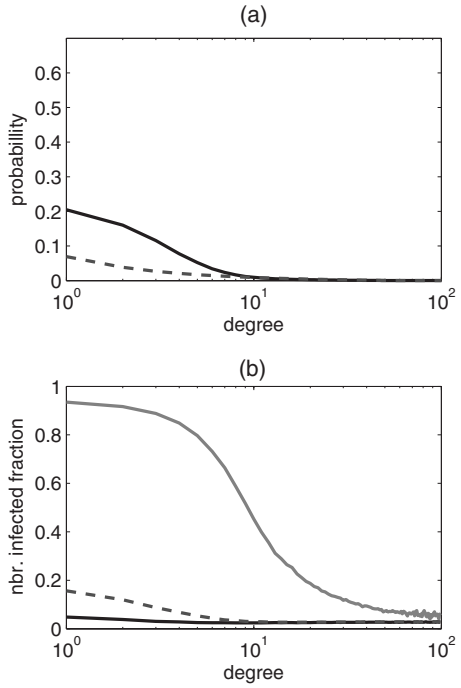

FIG. 5. (a) Actual (black line) and predicted (dashed gray line) degree distributions for infecteds. (b) Average fraction of neighbors that are infected vs degree. Solid gray line: infecteds; dashed line: recovereds; and black line: susceptibles. $p=0.002$, $q=0.0016$, $r=0.002$, and $w=0.04$.

$$k'' = w\frac{P_{SI} + P_{IR}}{P_{SI} + P_{IR} + 2P_{II}} \tag{15}$$

is the per link rewiring rate for links connecting to an infective (i.e., the ratio between links that can potentially rewire and total links into infectives). Figure 5(a) compares the actual degree distribution for infectives with the distribution predicted by Eq. (14). The number of low degree infectives is significantly overpredicted. This occurs because the mean field approximation in Eq. (15) is not accurate for infectives. Figure 5(b) shows the fraction of infected neighbors that a node has, depending on its degree and disease status. Results are averaged over 3×10^4 MCS. Low degree infected nodes tend to have a much higher fraction of neighbors that are also infected, due to transmission of the disease. Once infected, these neighbors will not rewire away until recovered, so the rewiring rate per link is smaller than one would expect from the mean field k'' in Eq. (15). Predicting the infective degree distribution accurately would require a theory that accounts for these correlations in infection status of neighboring nodes, which is beyond the scope of the present work.

B. Distance from an infective

We next consider the distribution of distances from a given node to the nearest infective. These distances are of interest because they relate to the number of hops the disease must make in order to reach an uninfected individual. The disease cannot propagate through recovered nodes until they become susceptible again, so the distance from the nearest

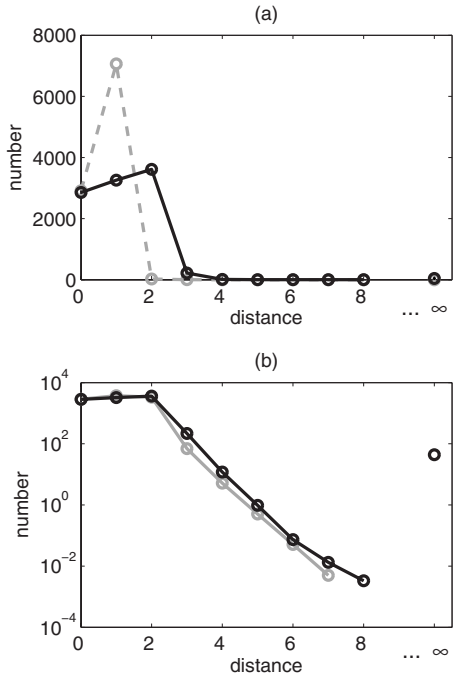

FIG. 6. Distribution of distances from the nearest infected node. ∞ indicates nodes that are completely disconnected from an infective. (a) Solid black line: with rewiring ($w=0.04$, $p=0.002$, and $q=0.0016$); dashed gray line: no rewiring ($w=0$, $p=0.002$, and $q=0.0009$). (b) Black line: rewired case [same as in (a)]; and gray line: distribution for random graphs, as described in text.

infective does not necessarily correspond to a path for disease propagation. However, we note that rewiring acts only on links to infectives, and thus the chains of susceptible and recovered links that this metric identifies will persist until the infection leads to their interruption. Figure 6(a) shows the distribution of distances from the nearest infective in the presence and absence of rewiring. To display the effect on the network geometry alone, rather than on the steady state number of infections as well, we have used a smaller q value for the $w=0$ case so that the total number of infectives is approximately the same in both curves. Results were averaged over 3×10^4 MCS, sampled every 100 MCS after removing transients. Rewiring significantly decreases the number of nodes that are directly connected to an infective. However, despite the rewiring, only a small fraction of nodes are fully disconnected from the infection.

Figure 6(b) shows a semilog plot of the $w=0.04$ case to display the tail of the curve at larger distances. An approximation based on random networks is also shown. Given how far from Poisson the degree distributions are when the network is rewired, it is somewhat surprising that the form of the decay in the distribution of distances can be predicted from random networks. Beginning with S, I, and R nodes in numbers matching that observed in the average of Monte Carlo simulations, we generated 1000 random networks and added randomly selected links until the number of S-S, S-I, S-R, etc. links also matched that from the average of Monte Carlo simulations. As Fig. 6(b) shows, the distribution of distances for these random networks decays in the same way as it does in an adaptive network. Thus the form of the distribution of distances depends mainly on local dynamics (node and link dynamics) rather than on the details of longer range correlations. The main difference is that the adaptive network has some nodes fully disconnected from infected components, while the random networks do not. Most of these nodes are recovereds with degree 0, which appear when infectives of degree 0 recover. Each type of node in the random networks has a Poisson degree distribution, so they do not generally have nodes of degree 0.

V. FLUCTUATIONS AND OTHER DYNAMICS

In the previous sections, we have considered steady states and long time averages of network properties. We next consider fluctuations and dynamical properties of the endemic state.

A. Fluctuations near bifurcation point

Near the bifurcation point where the endemic state loses stability, the number of infectives has larger fluctuations due to noise overcoming weak attracting forces [22]. Fluctuations in the SIRS model are significantly larger than those in the previously studied SIS model. We quantify the fluctuations by computing the standard deviation divided by the mean for long time series in both the Monte Carlo and mean field simulations. In Fig. 7, we plot the fluctuations as the infection rate p is swept toward the bifurcation point. Monte Carlo results were computed from 5×10^5 MCS time series sampled every ten MCS, except for the two smallest p values, for which shorter time series were used due to the shorter lifetimes of these states. All time series were longer than 10^5 MCS.

For comparison, the mean field equations can also be considered near equilibrium in stochastic form. In general, near equilibrium fluctuations can be modeled as additive noise [23], and we do so here. (We do note that multiplicative noise effects generate results similar to those reported for additive noise.) We assume the mean field is of the following form:

$$\mathbf{X}' = \mathbf{F}(\mathbf{X}) + \epsilon\eta(\mathbf{t}), \tag{16}$$

where $\mathbf{F}(\mathbf{X})$ is the mean field system in Eqs. (1)–(9), and $\langle\eta(\mathbf{t})\eta(\mathbf{t}')\rangle=\delta(t-t')$. ϵ is the noise strength, or amplitude. We have considered both additive noise and multiplicative noise cases in the simulations of the stochastic attractors near the endemic state and have computed the standard deviation divided by the mean as described above for ten random initial conditions near equilibrium and ten realizations.

We recall from Figs. 2 and 3 that depending on the value of the resusceptibility rate q, the bistability regions III are vastly different. Specifically, for $q=0.0016$, we saw that for sufficiently large wiring rates, the saddle–saddle and Hopf bifurcation branches were well-separated, whereas for $q=0.0064$, the branches were very close for small values of rewiring rate w. In Monte Carlo simulation, we have not observed the Hopf bifurcations or stable periodic oscillations seen in the mean field, even for system sizes as large as 4×10^5 nodes. Although the value of $q=0.0064$ we use in the

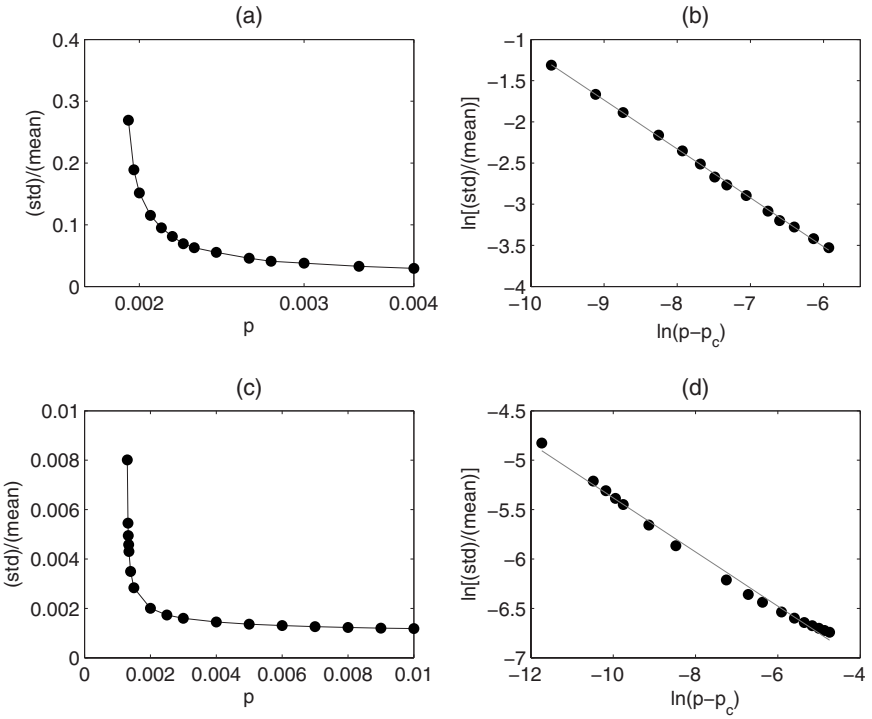

FIG. 7. Fluctuations in infectives (standard deviation divided by mean) vs infection rate p near the bifurcation point: (a) Monte Carlo and (b) mean field. Curves are to guide the eye. Log-log plots (data points with best fit lines) show power law scaling for both Monte Carlo (b) and mean field (d). Monte Carlo parameters: $q=0.0016$, $w=0.04$, and $r=0.002$. Mean field parameters: $q=0.0064$, $w=0.04$, $r=0.002$, and $\epsilon=0.0001$.

mean field fluctuation study is different from that used in the Monte Carlo, the local bifurcation structure is similar when $w=0.04$, in that it is a true saddle-node bifurcation point. This has been checked by examining the local linear vector field at the saddle-node point in question. Therefore, although the mean field has different q value, the bifurcation structure is equivalent to that observed in Monte Carlo simulation, so we use $q=0.0064$ in the fluctuation study.

The computations reveal that the fluctuations exhibit power law scaling, as shown in the log-log plots of Figs. 7(b) and 7(d). On the horizontal axis, we plot $\ln(p-p_c)$, where p_c is the critical point at which the endemic state loses stability. For the mean field, the bifurcation point is known exactly by examining the eigenvalues of the linearized vector field at the steady state. We approximate the Monte Carlo bifurcation point p_c as the value that produces the most linear plot. Although both cases have power law scaling, the exponents are different: −0.59 for Monte Carlo and −0.27 for mean field. The scaling exponent for the full system depends on the number of nodes. Whether it will approach the mean field value in the limit of infinite system size is a subject for further study. We note that fluctuations near a Hopf bifurcation point, as occurs in the mean field for $q=0.0016$, would produce a very different form of scaling from the saddle-node case. One of the reasons for the difference is that the instability is then two-dimensional and underdamped [24]. This is known to cause very different scaling laws in generic problems, which can be much slower [25].

To motivate the power law scaling of the fluctuations, we consider scaling near a generic saddle-node bifurcation. The simplest generic case of a saddle-node bifurcation for equilibrium points comes from solving for zeroes of the vector field at a parameter value where one eigenvalue of the Jacobian passes through zero. Standard normal form analysis allows one to consider the generic problem of a saddle-node bifurcation. In one dimension, the stochastic differential equation of a saddle-node bifurcation may be modeled as

$$dx_t = (a - x_t^2)dt + \sigma dW_t. \tag{17}$$

The parameter is a, and we suppose noise is additive. Since noise in general may cause a "shift" in parameter values where the saddle-node point disappears, we assume that the noise near the bifucation is sufficiently small, where dW/dt is a white noise term, and dW is a Brownian increment.

We further assume that we are always near the attracting branch of the saddle node, so we are in a near equilibrium setting. Such an assumption allows us to examine the stationary probability density function (PDF) of the stochastic dynamics by employing the Fokker-Planck equation near steady state. For the stochastic differential equation, Eq. (17), the PDF is well known [22] and is given by

$$p(a,x,\sigma) = Ne^{2(ax-x^3/3)/\sigma^2}. \tag{18}$$

Here N is a normalization constant. We compute the first and second order moments directly using Eq. (18) and then take the ratio of the standard deviation to the mean. Since $a=0$ is the value of the saddle-node point, we examine the fluctuations in the neighborhood of that value. The results, shown in Fig. 8, display power law scaling.

B. Delayed outbreaks

We next consider phase relationships between the fluctuating variables. We tracked the number of infectives in the system at each time point as well as the number of nodes that neighbored an infective (i.e., the number of SI and IR links). In the rewired system, fluctuations in the number of infectives lagged behind fluctuations in the number of infective neighbors that are not themselves infected, as shown in Fig. 9(a).

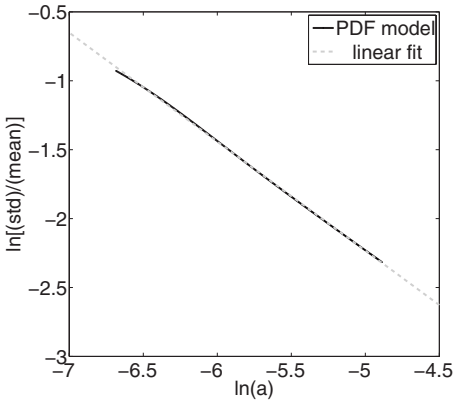

FIG. 8. Fluctuation size of a generic saddle-node bifurcation as a function of bifurcation parameter a near the bifurcation point using Eq. (18). The noise level used is 0.005.

Both mean field and Monte Carlo simulations of the full system displayed this effect, and we studied their dependence on the rewiring rate. Monte Carlo simulations were sampled every 1 MCS for 3×10^4 MCS after discarding transients. The mean field was sampled every 1 time unit for 5×10^4 units. Additive noise was included in the mean field equations with noise strength $\epsilon=0.0001$. Cross correlations between the infectives and the infective neighbors were computed for varying shifts between the time series, and the lag maximizing the cross correlation was identified. As shown in

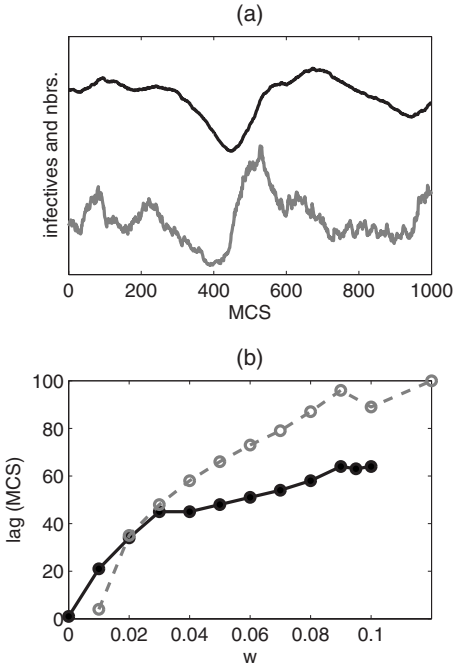

FIG. 9. Delayed outbreaks due to rewiring. (a) Monte Carlo time series. Black line: infectives and gray line: neighbors of infectives. Curves are scaled in arbitrary units for comparison of peak times. $p=0.0065$, $w=0.09$, $q=0.0016$, and $r=0.002$. (b) Time in MCS by which infectives lag behind infective neighbors vs rewiring rate. Solid black line: Monte Carlo and dashed gray line: mean field. $p=0.0065$, $q=0.0016$, $r=0.002$, mean field noise strength $\epsilon=0.0001$.

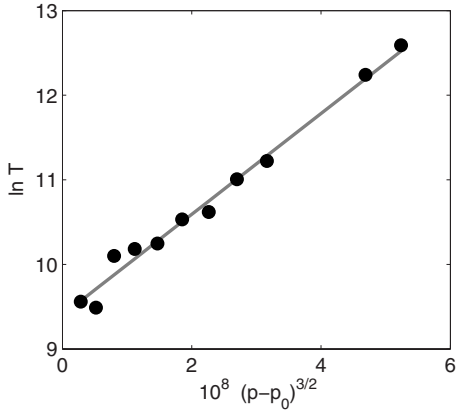

FIG. 10. Dependence of endemic state average lifetimes on infection rate p. Points: Monte Carlo simulations; line: best fit line. $q=0.0016$, $r=0.002$, and $w=0.04$. See text for details.

Fig. 9(b), rewiring leads to increasing lag times and delayed outbreaks. We also computed time lags for the mean field model with multiplicative noise and found the same trend of increasingly delayed outbreaks with larger rewiring.

C. Lifetime of endemic steady state

The final dynamic effect we consider is the lifetime of the endemic steady state. Because the system is stochastic and the disease-free state is absorbing, all parameter values will lead to eventual die out of the disease in the infinite time limit. These lifetimes become shorter and die out is more easily observed in the bistable regime near the bifurcation point where the endemic state has weak stability. We measured the dependence of the lifetimes on the infection rate p. For each p value, we prepared a steady state initial condition and computed multiple duplicate runs to obtain a distribution of lifetimes. (We computed 100 duplicate runs for all but the two highest p values and over 25 runs for the two highest.) We then calculated the average lifetime T for each p. For a generic saddle-node bifurcation in one dimension, it is expected that $\ln T$ is a linear function of $(p-p_0)^{3/2}$, where p_0 is the bifurcation point [26,27]. We obtained spurious results for our system with 10^4 nodes, possibly because the small system size led to rapid die out and we were unable to obtain good statistics near the bifurcation point. Away from the bifurcation point, the system has a weakly damped oscillatory component and behaves like a focus. By switching to a system with 4×10^4 nodes and 4×10^5 links, we were able to run longer simulations closer to the bifurcation point and operate in a regime where only one dimension mattered and the oscillations could be ignored. Preliminary scaling results are shown in Fig. 10. We used the bifurcation point p_0 that gave the best fit line, which led to an R value of 0.99. The scaling results appear consistent with expectations, but further study and better statistics are needed.

VI. CONCLUSIONS AND DISCUSSION

We have explored the stable states, network properties, and dynamics of an SIRS model on a network with adaptive

rewiring. As with the SIS model studied previously by Gross *et al.* [19], the rewiring leads to bistability of the endemic and disease-free states. A mean field version of the model predicted the steady states with good numerical accuracy and was also valuable in studying the fluctuations of the system, with the caveat that one must be near the appropriate type of bifurcation in the mean field to obtain corresponding results. With the addition of the recovered class and resusceptibility rate, we can control the width of the bistability region by manipulating the location of the bifurcation points.

The fluctuations in the infectives near the bifurcation point showed power law scaling. This agreed with mean field results and our expectations for scaling near a saddle-node bifurcation.

We studied the effects of the rewiring on the network geometry. Degree distributions were altered, and mean field arguments were able to predict the distributions for susceptibles and recovereds. However, a new analytical approach that includes correlations is needed to fully understand the degree distributions.

The other network property we considered was the distribution of distances from noninfected nodes to the nearest infective, a quantity that may be important in disease spreading and its control. This distribution depended primarily on node and link dynamics rather than on higher order correlations, so it could be predicted from random graphs. It is possible to compute the distribution of distances from an infective analytically for random graphs, but this calculation is awkward for a three species system (S, I, R) and does not have a simple functional form, so we have omitted the discussion of analytical results here.

Delayed outbreaks were observed in the rewired system. Peaks in the infective fraction lagged behind peaks in the number of nodes that neighbor an infective. For the parameter values studied here, the lag time is on the order of 10% of the mean infectious period, which might be considered a very short lag time. However, the parameters in this study were not selected to correspond to any specific disease. For most real diseases, we would expect a much slower rate for immunity to wear off and recovered individuals to become susceptible again, compared to the mean infectious period. This regime would be more difficult to study in Monte Carlo simulations, since the average number of infected nodes would be much smaller than seen here. Further work is needed to determine whether the observation of delayed outbreaks due to rewiring would persist or perhaps become more significant in a physically realistic system.

Finally, we considered lifetimes of the endemic state near the saddle-node bifurcation where it loses stability. In order to achieve extinction from a steady state, the disease must first overcome the attractive forces, which are weak near the bifurcation point. Due to the generic local topology of the saddle-node structure, the escape rate is well-characterized analytically [25]. We found that the Monte Carlo simulation agrees qualitatively with the escape times and yields a well-known power law. However, this is for parameters in which endemic and extinction states are not too far apart. Such extinction regimes can be analyzed using a Fokker-Planck approach [28]. Although preliminary results are in agreement with the expected scaling, further study of the lifetime scaling is needed, including in regimes that are physically realistic, and where the usual extinction rates cannot be modeled with a Fokker-Planck approach.

In addition to the directions for further research mentioned above, a major challenge is to develop network geometries and rewiring rules that are more consistent with human social networks. Real social networks are expected to have community structure [29]. The networks studied here did not. In our rewired networks, the number of connections from noninfected nodes to infected nodes was reduced in comparison to a random network, while the number of connections between noninfected nodes was increased. However, this process does not induce a community structure on the network in the Newman-Girvan Q-modularity sense [30]. Rewiring was a nonlocal effect; new neighbors were chosen at random among all noninfected nodes in the network rather than introducing a local structure. It has been shown for static networks that community structure affects disease dynamics [31,32], and we expect an impact in adaptive networks as well.

In the current work, an ideal setting was proposed where noninfected nodes were assumed to behave rationally and have perfect knowledge of the disease status of their current neighbors and potential new neighbors. It would be of interest to consider a situation in which not all contagious individuals appear ill or know that they are contagious, as might be the case for a sexually transmitted disease possessing asymptomatic individuals. This effect might be modeled by simultaneous spreading through the network of both the disease and information about the disease. If the current model is extended with information and community structure, social dynamics could be extrapolated to improve contact tracing and epidemic control in organized populations with local structure.

ACKNOWLEDGMENTS

This work was supported by the Office of Naval Research, Center for Army Analysis, and Armed Forces Medical Intelligence Center. The authors wish to thank Thilo Gross, Bernd Blasius, Royce Zia, and Mark Dykman for helpful discussions.

[1] R. M. Anderson and R. M. May, *Infectious Diseases of Humans* (Oxford University Press, New York, 1991).
[2] J. Verdasca, M. M. Telo Da Gama, A. Nunes, N. R. Bernardino, J. M. Pacheco, and M. C. Gomes, J. Theor. Biol. **233**, 553 (2005).
[3] M. J. Keeling, *Ecology, Genetics, and Evolution* (Elsevier, New York, 2004).
[4] J. P. Aparicio and H. G. Solari, Math. Biosci. **169**, 15 (2001).
[5] M. S. Bartlett, J. R. Stat. Soc. Ser. B (Methodol.) **11**, 211 (1949).
[6] L. Billings and I. B. Schwartz, Phys. Lett. A **297**, 261 (2002).
[7] R. W. West and J. R. Thompson, Math. Biosci. **141**, 29 (1997).
[8] D. A. Cummings *et al.*, Proc. Natl. Acad. Sci. U.S.A. **102**, 15259 (2005).
[9] J. A. Jacquez and C. P. Simon, Math. Biosci. **117**, 77 (1993).
[10] R. Pastor-Satorras and A. Vespignani, Phys. Rev. E **63**, 066117 (2001).
[11] M. Kuperman and G. Abramson, Phys. Rev. Lett. **86**, 2909 (2001).
[12] Y. Moreno, R. Pastor-Satorras, and A. Vespignani, Eur. Phys. J. B **26**, 521 (2002).
[13] C. Moore and M. E. J. Newman, Phys. Rev. E **61**, 5678 (2000).
[14] L. Hufnagel, D. Brockmann, and T. Geisel, Proc. Natl. Acad. Sci. U.S.A. **101**, 15124 (2004).
[15] D. H. Zanette and M. Kuperman, Physica A **309**, 445 (2002).
[16] R. A. Kosinski and L. Adamowski, Int. J. Mod. Phys. C **15**, 755 (2004).
[17] N. H. Fefferman and K. L. Ng, Phys. Rev. E **76**, 031919 (2007).
[18] E. Volz and L. A. Meyers, Proc. R. Soc. London, Ser. B **274**, 2925 (2007).
[19] T. Gross, Carlos J. Dommar D'Lima, and B. Blasius, Phys. Rev. Lett. **96**, 208701 (2006).
[20] D. H. Zanette and S. R. Gusmán, e-print arXiv:0711.0874.
[21] E. J. Doedel, R. Paffenroth, A. Champnets, T. Fairgrieve, Y. A. Kuznetsov, B. Sandstede, and X. Wang, AUTO: Software for continuation and bifurcation for ordinary differential equations (2001).
[22] W. Horsthemke and R. Lefever, *Noise-Induced Transitions: Theory and Applications in Physics, Chemistry, and Biology*, Springer Series in Synergetics Vol. 15 (Springer, New York, 1983).
[23] N. G. Van Kampen, *Stochastic Processes in Physics and Chemistry*, 3rd ed. (Elsevier, Amsterdam, 2007).
[24] L. Arnold, *Random Dynamical Systems* (Springer, New York, 2001).
[25] M. I. Dykman, I. B. Schwartz, and M. Shapiro, Phys. Rev. E **72**, 021102 (2005).
[26] M. I. Dykman and M. A. Krivoglaz, Physica A **104**, 480 (1980).
[27] R. Graham and T. Tél, Phys. Rev. A **35**, 1328 (1987).
[28] C. Doering *et al.*, Multiscale Model. Simul. **3**, 283 (2005).
[29] M. Girvan and M. E. J. Newman, Proc. Natl. Acad. Sci. U.S.A. **99**, 7821 (2002).
[30] M. E. J. Newman and M. Girvan, Phys. Rev. E **69**, 026113 (2004).
[31] A. Grabowski and R. A. Kosinski, Phys. Rev. E **70**, 031908 (2004).
[32] W. Huang and C. Li, J. Stat. Mech.: Theory Exp. (2007) P01014.